

The influence of reflections from the train body and the ground on the sound radiation from a railway rail

Reflections
from the train
body and the
ground

1

David J. Thompson, Dong Zhao, Evangelos Ntotsios and
Giacomo Squicciarini

*Institute of Sound and Vibration Research, University of Southampton,
Southampton, UK*

Ester Cierco

Ingeniería para el Control del Ruido SL, Barcelona, Spain, and

Erwin Jansen

TNO Acoustics and Sonar, Den Haag, The Netherlands

Received 8 November 2023
Revised 13 December 2023
Accepted 15 December 2023

Abstract

Purpose – The vibration of the rails is a significant source of railway rolling noise, often forming the dominant component of noise in the important frequency region between 400 and 2000 Hz. The purpose of the paper is to investigate the influence of the ground profile and the presence of the train body on the sound radiation from the rail.

Design/methodology/approach – Two-dimensional boundary element calculations are used, in which the rail vibration is the source. The ground profile and various different shapes of train body are introduced in the model, and results are observed in terms of sound power and sound pressure. Comparisons are also made with vibro-acoustic measurements performed with and without a train present.

Findings – The sound radiated by the rail in the absence of the train body is strongly attenuated by shielding due to the ballast shoulder. When the train body is present, the sound from the vertical rail motion is reflected back down toward the track where it is partly absorbed by the ballast. Nevertheless, the sound pressure at the trackside is increased by typically 0–5 dB. For the lateral vibration of the rail, the effects are much smaller. Once the sound power is known, the sound pressure with the train present can be approximated reasonably well with simple line source directivities.

Originality/value – Numerical models used to predict the sound radiation from railway rails have generally neglected the influence of the ground profile and reflections from the underside of the train body on the sound power and directivity of the rail. These effects are studied in a systematic way including comparisons with measurements.

Keywords Rolling noise, Sound radiation, Railway track, Boundary elements, Ground reflections, Directivity

Paper type Research paper

© David J. Thompson, Dong Zhao, Evangelos Ntotsios, Giacomo Squicciarini, Ester Cierco and Erwin Jansen. Published in *Railway Sciences*. Published by Emerald Publishing Limited. This article is published under the Creative Commons Attribution (CC BY 4.0) licence. Anyone may reproduce, distribute, translate and create derivative works of this article (for both commercial and non-commercial purposes), subject to full attribution to the original publication and authors. The full terms of this licence may be seen at <http://creativecommons.org/licenses/by/4.0/legalcode>

This work has been supported by the TRANSIT project (funded by EU Horizon 2020 and the Europe's Rail Joint Undertaking under Grant Agreement 881771). The contents of this paper only reflect the authors' views; the Joint Undertaking is not responsible for any use that may be made of the information contained in the paper.



1. Introduction

Rolling noise, radiated by the vibration of the wheels and track, is the dominant source of noise from railway operations at conventional speeds, and remains important up to speeds exceeding 300 km/h. The wheel radiation is usually the main component above 2 kHz, whereas the radiation from the rails dominates the important mid-frequency region between 400 and 2000 Hz, and the sleepers contribute most to the low frequency noise (Thompson, 2009).

In early analytical modeling of rolling noise (Remington, 1976a, 1976b), the model of Bender and Remington (1974) was used for the sound radiation from the rail. This calculated the radiation efficiency for both vertical and horizontal motions using a model of an oscillating cylinder, which was located in a free field. A uniform directivity was assumed, which showed reasonable agreement with directivity measurements on a 6 m length of rail laid on rubber pads. Subsequently the noise propagation was modified by including the ground, modeled as a finite impedance plane (Remington, 1987).

Since the early 1990s, the TWINS model has become widely used to predict rolling noise (Thompson, Hemsforth, & Vincent, 1996; Thompson, Fodiman, & Mahé, 1996). This contains a series of numerical and analytical models for the vibration and sound radiation of the wheels, rails and sleepers. For the sound radiation from the rail, an equivalent source model was used, based on an approximate geometry of the rail cross-section (Petit, Heckl, Bergemann, & Baae, 1992); as in Bender and Remington (1974), the rail was modeled in free space. Similar results were obtained by using a two-dimensional (2D) boundary element (BE) model of the rail radiation in free space (Thompson, 1988; Thompson, Jones, & Turner, 2003).

The validity of using such a two-dimensional approach was investigated (Thompson *et al.*, 2003) using an equivalent line of point sources that accounted for the wave propagation in the rail. It was shown that, due to the long wavelengths and low decay rates of rail vibration, a 2D model gave acceptable results in most practical cases for frequencies above about 250 Hz. At lower frequencies, the radiation resembled that from a point source instead of a line source.

In reality, the rail is located in close proximity to the ground. Zhang, Squicciarini, and Thompson (2016) found that the radiation efficiency is significantly affected by the presence of the ground at frequencies below 1 kHz. Different 2D BE models were considered for a rail located on the ground, representing the sleepers, or a rail above the ground, representing for example the ballast between the sleepers. It was shown by Zhang, Thompson, Quaranta, and Squicciarini (2019) that the overall sound power from the rail can be estimated using a combination of these two models. However, this approach has not been used to study the sound pressure at the trackside.

Van Lier (2000) modeled the radiation of an embedded rail using 2D finite elements (FE), whereas Han, He, Wang, and Xiao (2021) used a 3D BE model to calculate the sound radiated from an embedded rail. Nilsson, Jones, Thompson, and Ryue (2009) studied the sound radiation from both an open rail and an embedded rail using a combination of waveguide FE and wavenumber BE (also called 2.5D methods). Ryue, Jang, and Thompson (2018) extended this approach to include reflections from a ground plane with a finite impedance and presented results in terms of directivities as well as radiation efficiencies.

Theysen (2022) used a waveguide FE/BE method to calculate the sound radiation from a rail, and allowed for the inclusion of a rigid ground and a car body structure. Acoustic transfer functions were precalculated and used in the simulation of time-domain sound pressure signals during a train passage.

Measurements of directivity from a rail installed in a track were presented by Thompson (2009). For excitation in the vertical direction, the radiation was found to be slightly greater in the vertical direction than that in the lateral direction, whereas for excitation in the lateral direction, the reverse is true. However, for simplicity in the TWINS model (Thompson, Hemsforth, & Vincent, 1996), the directivity for vertical motion was approximated by a line

monopole, and that for lateral motion by a line dipole. The influence of ground reflections was added using an image source. Nevertheless, treating the ground as a horizontal plane, as commonly used in prediction models, involves simplifications (Dragna, Blanc-Benon, & Poisson, 2014).

Dittrich, Letourneaux, and Jones (2019) used a ray tracing approach to estimate the propagation of sound from the wheel and rail, represented as point sources, allowing for more complex ground topology. The results were expressed as the sound pressure level normalized by the equivalent sound power per unit length of the source, $L_p - L_{W'}$, allowing use in environmental noise calculations.

Zhang and Jonasson (2006) and Zhang (2010) presented measured directivities of the rail and wheel in both vertical and horizontal planes and showed that these can be approximated by a combination of monopole and dipole components. Using a mock-up of a car body, it was shown that the directivity of the wheel in a vertical plane is affected by the presence of the car body.

The aim of the present study is to quantify the influence of the ground profile and the scattering effect of the train body on the sound radiation from the rail. To study these effects, results from two-dimensional BE models are presented in Section 2, initially without the train present. The ballast profile of the track is introduced, and reflections from the ground are included by using an image receiver approach. In Section 3, the train body is introduced in the model, and comparisons are made with vibro-acoustic measurements carried out with and without a train present. In Section 4, results are presented for different shapes of train body, including the effect on the sound power as well as the sound pressure. Finally, in Section 5, the results obtained including the train body are compared with simple line source estimates of directivity to test the validity of this engineering approach.

There are two important practical applications of this work. The first is that it allows the influence of the car body on the directivity of sound radiated by the rail to be taken into account in rolling noise estimates. The second is related to experimental methods used to separate wheel and rail contributions to rolling noise (Thompson *et al.*, 2018). Ideally, the necessary vibro-acoustic transfer functions of the track should be measured with the train present, but for simplicity in these measurements, it is desirable to measure them without the train. If the difference between these two situations is known, it could be used as a correction applied to measurements undertaken without the train.

2. Boundary element models for sound radiation from the track

2.1 BE model for the track

The noise radiated by the rail is calculated using a 2D BE model. In BE acoustic analysis, only the surfaces surrounding the acoustic domain are discretized; this is more efficient than FE analysis, which requires a full mesh of the domain. Moreover, the far-field Sommerfeld boundary condition is included directly. The theory of acoustic BE analysis is described in detail by Wu (2000) and not reproduced here. Thompson *et al.* (2003) showed that 2D models give acceptable results for the noise from the rail above about 250 Hz, which is the region where the track decay rate is usually low. In this frequency region, which is generally well above the critical frequency of bending waves in the rail, the sound radiated by the rail propagates in a direction that is approximately perpendicular to its axis, so the sound field is 2D in nature.

The geometry of the model for the track is depicted in Figure 1. The train body has not been included in these initial calculations. Two models of the track have been used. In the first model, the rails (UIC60) are attached directly to the upper surface of the sleeper. The sleeper surface is treated as rigid, whereas the region beside the sleepers has been assigned an acoustic impedance boundary condition representative of ballast. The impedance has been

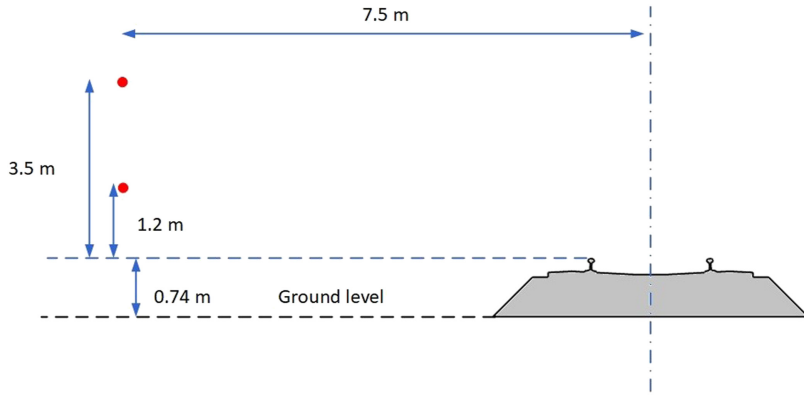


Figure 1.
Schematic view of the
BE model of the track

Source(s): Authors' own work

defined according to [Delany and Bazley \(1970\)](#), using an equivalent flow resistivity of 5×10^5 Pa.s/m². The second model corresponds to the region between sleepers; here, the rail foot is located at a height of 62.5 mm above the ground, and in this model the whole surface of the track is modeled as ballast. The results from these two models have been combined, as in [Zhang et al. \(2019\)](#). The sound pressure is determined at receivers that are 7.5 m from the track centerline, and at a height of 1.2 m and 3.5 m above the rail head. Additionally, there are image receivers located at approximately 2.7 m and 5.0 m below the rail (the ground surface is omitted from the BE model). A unit velocity in the vertical or lateral direction is applied, first to one rail and then to the other.

The BE calculations have been carried out using the software WANDS ([Nilsson & Jones, 2007](#)), which has been verified by [Nilsson et al. \(2009\)](#) among others. A coarse BE mesh has been used for lower frequencies (up to 500 Hz), and a fine one for higher frequencies; in each case, it was ensured that there were at least six nodes per wavelength, so that the wave field is adequately resolved. As stated before, the ground plane was omitted from the BE model. In the model for lower frequencies, the 'image' of the track geometry below the level of the ground was also included in the mesh, but it was not required in the high frequency mesh. One-third octave band results were obtained, using four calculation points in each frequency band.

In [Figure 2](#), the sound power per unit length is shown for the current model and also for a free rail. These results are obtained for a unit velocity amplitude on the rail and show the same trends as [Zhang et al. \(2019\)](#).

To estimate the sound pressure at the receiver positions, the two solutions (for the rail attached to the sleepers and the rail above the ground) were combined using the same methodology as used in [Zhang et al. \(2019\)](#) to calculate the sound power. This gives the combined sound pressure amplitude $|p|^2$ as

$$|p|^2 = \begin{cases} \frac{b}{d}|p_m|^2 + \frac{(d-b)}{d}|p_q|^2 & \text{for } f > f_0 \\ \left| \left(\frac{b}{d} \right)^2 |p_m|^2 - \left(1 - \left(\frac{b}{d} \right)^2 \right) |p_q|^2 \right| & \text{for } f < f_0 \end{cases} \quad (1)$$

where $|p_m|^2$ is the squared pressure amplitude for the rail on the sleepers, $|p_q|^2$ is the squared pressure for the rail above the ground, b is the sleeper width and d is the spacing between

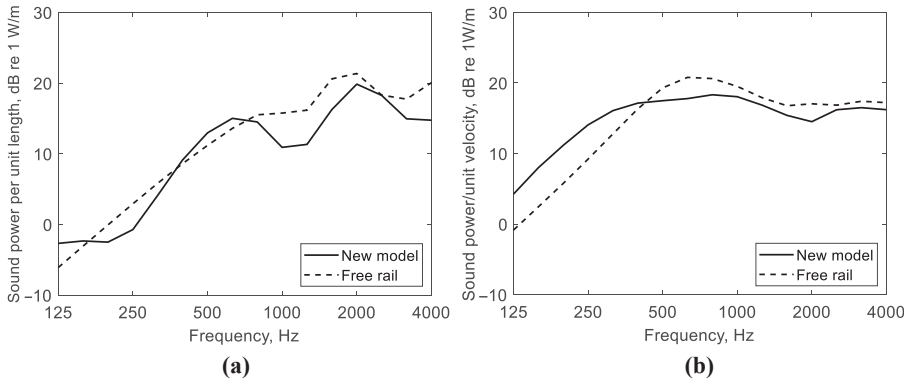


Figure 2.
Sound power per meter
for a unit velocity of
the rail

Note(s): (a) Rail vibrating vertically; (b) rail vibrating laterally
Source(s): Authors' own work

sleepers; values of $b = 0.2$ m and $d = 0.6$ m were used, unless otherwise stated. For vertical rail vibration, $f_0 = c_0/d$ with c_0 the sound speed. For lateral rail vibration, $f_0 = 0$, ensuring that the first equation is always used.

Figure 3 shows the spectra of sound pressure level from vertical and lateral rail vibration at the four receiver locations. Shielding by the ballast shoulder causes the sound to be attenuated at the positions below the ground level; without this shielding, the levels would be similar to those at the receivers above the ground. This is seen especially above 500 Hz for the radiation from vertical rail vibration, where there are differences of around 10 dB.

2.2 Line source estimates

For radiation from the vertical rail vibration, the directivity is expected to be similar to a line monopole (Thompson, Fodiman, & Mahé, 1996). In the presence of a rigid ground (spreading over a hemicylinder), this yields

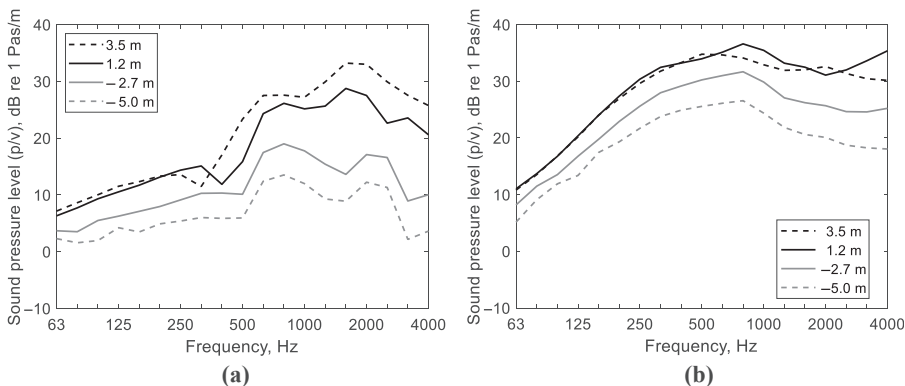


Figure 3.
Sound pressure
radiated by a unit
velocity on the rail;
receivers at 7.5 m
distance and different
heights – case without
ground

Note(s): (a) Rail vibrating vertically; (b) rail vibrating laterally
Source(s): Authors' own work

$$\Delta L = L_p - L_{W'} = -10 \log_{10} r - 5, \quad (2)$$

with r the distance to the receiver. This gives $\Delta L = -13.2$ dB for the receiver at 1.2 m height and $\Delta L = -13.7$ dB for the one at 3.5 m.

The results from Figure 3 are reproduced in the form $L_p - L_{W'}$ in Figure 4. The results for 1.2 m and 3.5 m heights in Figure 4(a) correspond well to the given estimates, apart from the dip around 400–500 Hz and a reduction above 2000 Hz. The results for the image source positions (heights -2.7 m and -5.0 m) are lower, again due to shielding from the ballast shoulder.

For radiation from the lateral rail vibration, the directivity is expected to be similar to a line dipole (Thompson, Fodiman, & Mahé, 1996). In the presence of a rigid ground, this yields

$$\Delta L = L_p - L_{W'} = -10 \log_{10} r - 5 + 10 \log_{10} (2 \cos^2 \theta), \quad (3)$$

with θ the angle to the horizontal. This gives $\Delta L = -10.3$ dB for the receiver at 1.2 m and $\Delta L = -11.7$ dB for the one at 3.5 m; again, these agree reasonably well with the results in Figure 4(b).

2.3 Inclusion of ground reflection

To obtain results including ground reflections, the free-field sound pressure amplitudes at the direct and image receiver positions are combined. For a partially absorptive ground, an amplitude reflection coefficient $R(\phi)$ is applied to attenuate the sound pressure amplitude at the image receiver location (Thompson, 2009). Assuming a locally reacting surface, $R(\phi)$ can be expressed as:

$$R(\phi) = \frac{(z'_n \cos \phi - 1)}{(z'_n \cos \phi + 1)} \quad (4)$$

where ϕ is the incident angle relative to the normal and $z'_n = z_n / \rho_0 c_0$, with z_n the acoustic impedance of the surface and ρ_0 the density of air. The angle ϕ can be calculated as

$$\phi = \frac{\pi}{2} - \tan^{-1} \frac{z_{\text{rec}} + z_{\text{srce}}}{|y_{\text{rec}} - y_{\text{srce}}|} \quad (5)$$

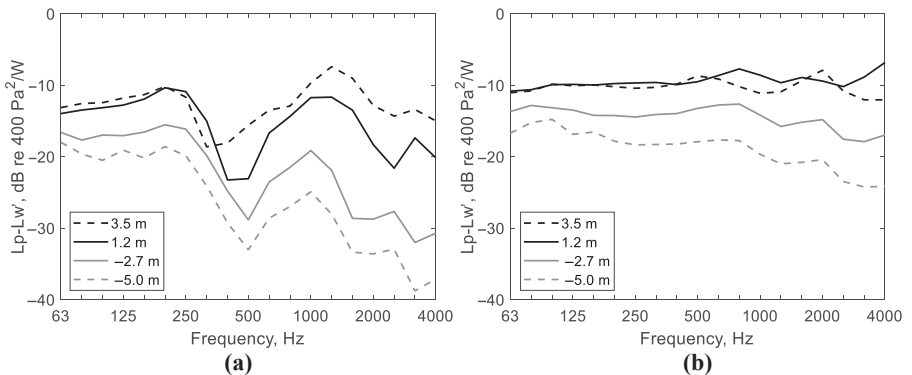


Figure 4.
Sound pressure level for a unit sound power level; receivers at 7.5 m and different heights – case without ground

Note(s): (a) Rail vibrating vertically; (b) rail vibrating laterally

Source(s): Authors' own work

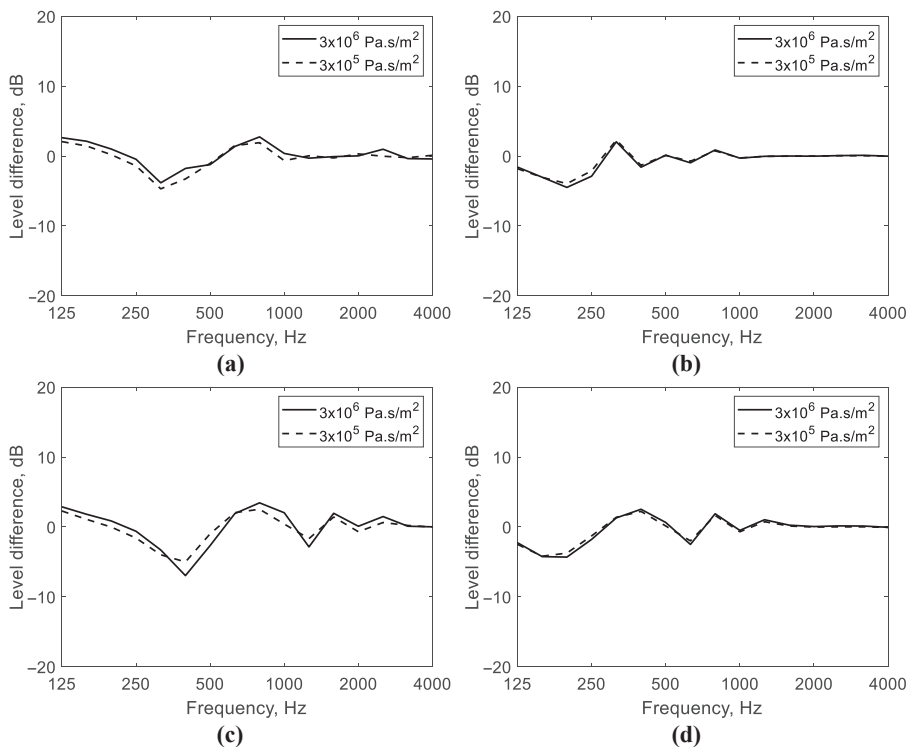
where z_{srce} and z_{rec} are the vertical coordinates of the source and image receivers, while y_{srce} and y_{rec} are their lateral coordinates. To determine this angle, the source position has been chosen to be at the top-left corner of the ballast shoulder as the rail itself does not have a direct line of sight to the image receiver.

Figure 5 presents the effect of including the ground in the form of a level difference, that is, the result including ground reflections minus the result with no ground. The ground impedance, z_n , has been estimated using Delany and Bazley (1970) with two values of equivalent flow resistivity. In both cases, the ground dip, at 300–400 Hz for the lower receiver and around 200 Hz for the upper one, is quite shallow due to the shielding effect of the ballast shoulder, without which a much deeper ground dip would be found. However, the introduction of the train body also affects the sound propagation, so this will be investigated in the next section.

3. Effect of train body

3.1 Measured transfer functions

To assess the effect of the presence of the car body, transfer function measurements have been performed on a ballasted track, both with and without a train being present on the track.



Note(s): (a) Rail vibrating vertically, 1.2 m receiver height; (b) rail vibrating vertically, 3.5 m receiver height; (c) rail vibrating laterally, 1.2 m receiver height; (d) rail vibrating laterally, 3.5 m receiver height

Source(s): Authors' own work

Figure 5. Sound pressure level difference due to including ground reflections, for receivers at 7.5 m distance

Further details of the measurements are provided in [Thompson, Dittrich, Jansen, Zhao, and Cierco \(2022\)](#).

Vibro-acoustic transfer functions were measured using two different methods. In the first method, transfer functions of the form p/F were measured, with p the sound pressure at 7.5 m from the track centre and F the force applied to the rail head. However, for practical reasons, these transfer functions were measured reciprocally ([Fahy, 1995](#)) by mounting an omnidirectional sound source at the receiver location and an accelerometer on the rail head. The transfer function a/\dot{q} was measured between the source volume acceleration \dot{q} and the vertical or lateral acceleration a of the rail. An average was used over different reciprocal source locations to allow for the line-source nature of the rail radiation. Measurements were performed at two cross-sections on the train: one in the bogie region, and the other near the centre of the vehicle. In the former case, the presence of the train will also cause differences in the rail vibration, which will affect the transfer function p/F .

In the second method, transfer functions of the form p/v , that is, sound pressure due to a unit velocity v of the rail, were measured using the advanced transfer path analysis (ATPA) method ([Magrans, 1981](#); [Thompson et al., 2018](#)). To achieve this, the track section was divided into subsections comprising two sleeper bays. Within each subsection, the acceleration of each rail in vertical and lateral directions and the vertical acceleration of the sleeper were treated as separate “subsystems”. When present, the wheels were also included as subsystems. Each subsystem was excited by a hammer at randomly distributed positions, and transmissibilities (ratios of acceleration at different points, a/a) were measured between each pair of subsystems. In the ATPA method, these are referred to as “global transfer functions” ([Magrans, 1981](#)). In addition, the sound pressure was measured at the receiver points and expressed as transfer functions of pressure divided by acceleration, p/a .

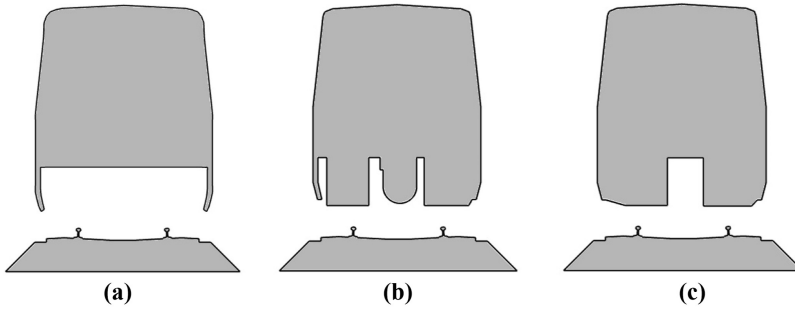
A matrix operation is used in the ATPA method to obtain the “direct transfer functions” $T_{k \rightarrow M}^D$, which express the sound pressure at a receiver point M due to vibration in one subsystem k when the response of all other subsystems is blocked ([Magrans, 1981](#)). For the rail, therefore, the direct transfer function corresponds to the pressure due to vibration of the rail in one subsystem while the sleepers and wheels are stationary. Because these are expressed relative to the average vibration in the subsystem, any change in the vibration due to the presence of the train will be allowed for.

3.2 BE models

For comparison with these measurements, the train body has also been added to the 2D BE model and represented using boundary elements. The metro train was represented by three different cross-sections, which are shown in [Figure 6](#). The track is ballasted, and the sleeper spacing in [Equation \(1\)](#) is set to 1 m for these calculations, chosen equal to that in the measurement situation.

Similar to the track model, a coarse BE mesh has been used for lower frequencies and a fine one for higher frequencies. In each case, there were again at least six nodes within an acoustic wavelength. The bottom surfaces of the train were assigned an impedance corresponding to an absorption coefficient of 0.2 at all frequencies ([Li et al., 2021](#)). The rest of the car body was modeled as rigid.

One rail at a time was assigned a unit vertical or lateral velocity amplitude; results are thereby obtained for both the near and far rails. As described earlier, results have been combined for configurations with the rail attached to the ground and the rail suspended above the ground, [Equation \(1\)](#). The sound pressure was determined for a receiver position at 7.5 m from the track and 1.2 m above the top of the rail. At the measurement site, the adjacent ground was covered in long grass and vegetation, so, to approximate an absorptive ground, the ground reflections were not considered in the model.



Note(s): (a) M1; (b) M2; (c) M3

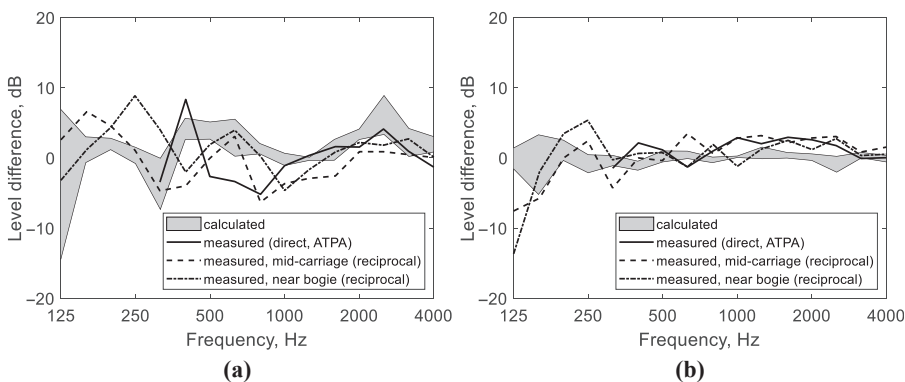
Source(s): Authors' own work

Figure 6.
Three train cross-sections used to represent metro train in 2D BE model

3.3 Comparison between measurements and calculations

In [Figure 7](#), the measured and predicted results are compared for vibration of the near rail. These are shown in the form of the sound pressure level with the train present minus the one without it. The predicted results show the range covered by the three train models in [Figure 6](#). For rail vibration in the lateral direction, [Figure 7 \(b\)](#), the predicted level difference is close to 0 dB; the measurements are in the range 0–2 dB above 300 Hz. For the vertical rail vibration, [Figure 7 \(a\)](#), the results exhibit greater variability with frequency as well as between the different measurements. In each case, there are only small differences between the predicted results for the three train profiles and they capture the main trends in the measurements.

[Figure 8](#) shows the corresponding results for vibration of the far rail; only the ATPA measurement was available in this case. The noise calculated from the rail is reduced by up to about 4 dB in the range 500–2000 Hz by the presence of the train body. Similar trends are seen in the measurements.



Note(s): Receiver distance 7.5 m and height 1.2 m above the rail; results for near rail.

(a) Rail vibrating vertically; (b) rail vibrating laterally

Source(s): Authors' own work

Figure 7.
Effect of introducing the metro train on the sound pressure level from the near rail, without ground

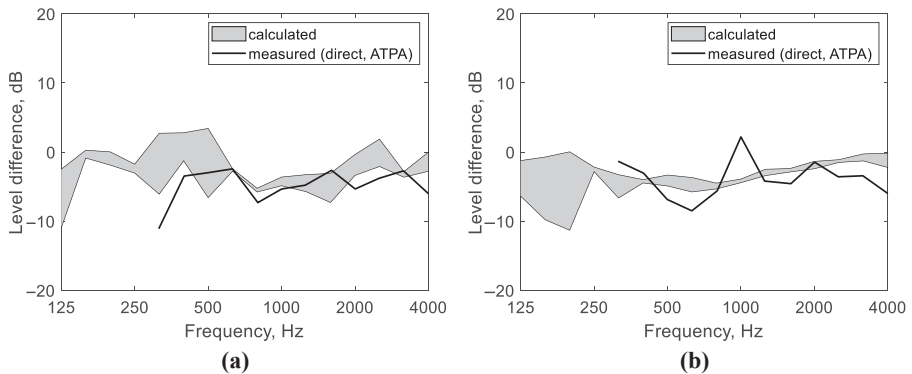


Figure 8.
Effect of introducing the metro train on the sound pressure level from the far rail, without ground

Note(s): Receiver distance 7.5 m and height 1.2 m above the rail; results for far rail. (a) Rail vibrating vertically; (b) rail vibrating laterally

Source(s): Authors' own work

3.4 Directivity

To give some insight into the effect of introducing the train body, the sound pressure has been calculated over a semicircle of radius 15 m centered at the middle of the track. The angular distribution of sound pressure level due to the vertical rail vibration is plotted in Figure 9. Results were calculated for angles spaced 5° apart, both with and without the train body. These were based on the train model M2, Figure 6 (b).

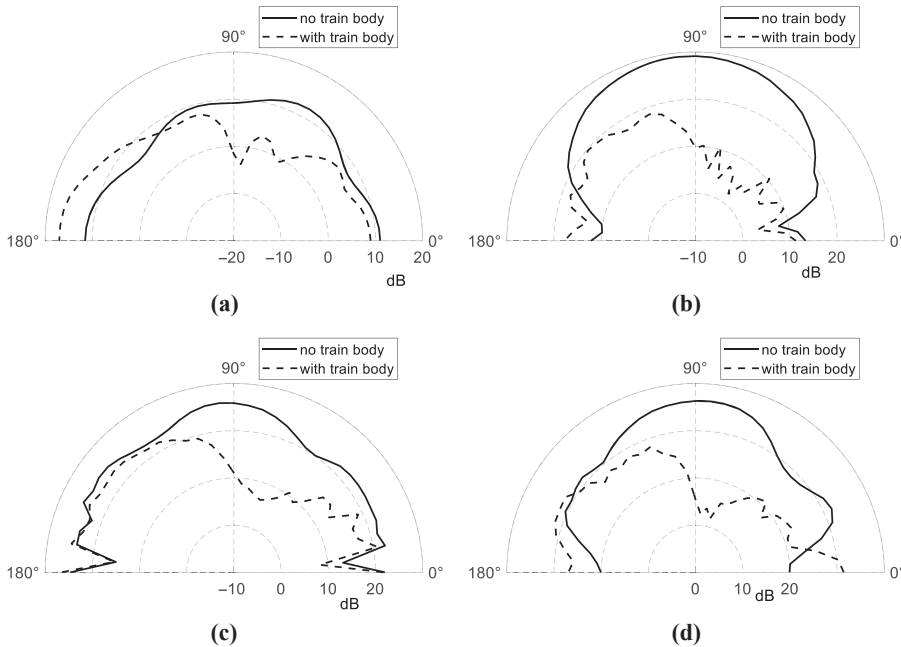
As would be expected, shielding by the train body causes a reduction in the radiation directly upward, especially toward the right-hand side when the left rail is excited. However, the sound radiated toward the sides is generally affected much less, as observed in Figures 7 and 8.

4. Results for different train geometries

To investigate the influence of the train profile, results are presented in this section from calculations for six different train cross-sections. These include the three profiles of the metro train considered earlier, shown in Figure 6, and three further profiles, depicted in Figure 10. Figure 10 (a,b) represents different cross-sections of a generic train with part of the bogie frame included, and Figure 10 (c) represents a high-speed train with a low curved floor. As before, the bottom surface of the train was assigned an impedance corresponding to an absorption coefficient of 0.2. In the calculations presented in this section, the sleeper spacing in Equation (1) was restored to $d = 0.6$ m.

Before considering the effect on the sound pressure, the change in the sound power due to introducing the different train profiles was determined. The results are shown in Figure 11. For the vertical vibration of the rail, the sound power is reduced by 2–6 dB above 200 Hz. As may be deduced from the directivity plots in Figure 9, this is mainly associated with the reflection of sound downward toward the ballast, as well as the absorption on the underside of the vehicle. The metro train profiles in Figure 6, which are in closer proximity to the track, give slightly larger reductions in sound power than the train profiles in Figure 10. For the radiation from the lateral vibration of the rail, the sound power level is reduced by only 0–2 dB, with smaller variations between train profiles and very little variation with frequency.

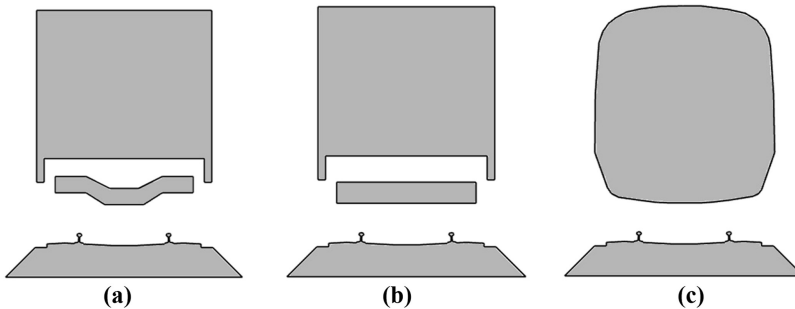
The corresponding results in terms of sound pressure level were calculated for the two receiver heights (1.2 m and 3.5 m) at 7.5 m from the track. Unlike the results presented in Section 3, the ground effect has been included in these results, based on a flow resistivity of



Note(s): Sound pressure due to unit vertical velocity of the left rail in one-third octave bands: (a) 125 Hz; (b) 500 Hz; (c) 1000 Hz; (d) 2000 Hz

Source(s): Authors' own work

Figure 9.
Angular distribution of
predicted sound
pressure level at 15 m
from the track center



Note(s): (a) B1; (b) B2; (c) HS

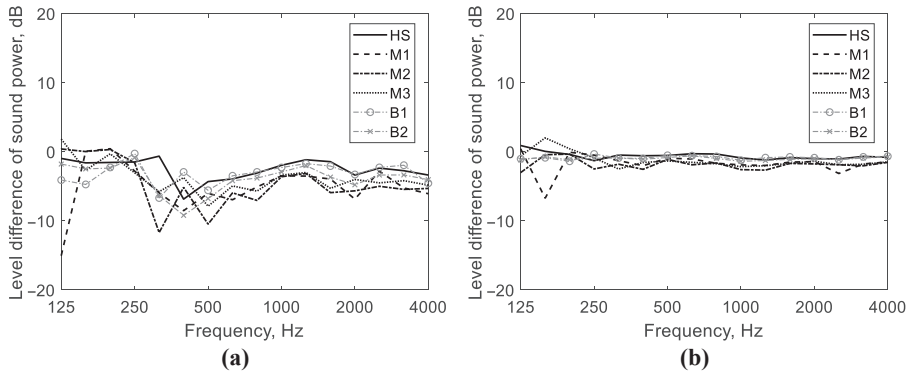
Source(s): Authors' own work

Figure 10.
Additional train
profiles considered

$3 \times 10^5 \text{ Pa.s/m}^2$. As indicated in Figure 1, the ground level was assumed to be 0.74 m below the rail. The results are shown in Figure 12 as the level difference between the cases with and without the train.

For radiation from the vertical vibration of the rail, the results show some variation with frequency and among the different train profiles. For the 1.2 m receiver height, Figure 12 (a), there is an increase in the noise level of 0–5 dB in most cases, with increases of up to 12 dB in the frequency bands 315–500 Hz. In this frequency region, the result without the train

Figure 11.
Change in the sound power level when the train body is introduced with different train profiles



Note(s): (a) Rail vibrating vertically; (b) rail vibrating laterally
Source(s): Authors' own work

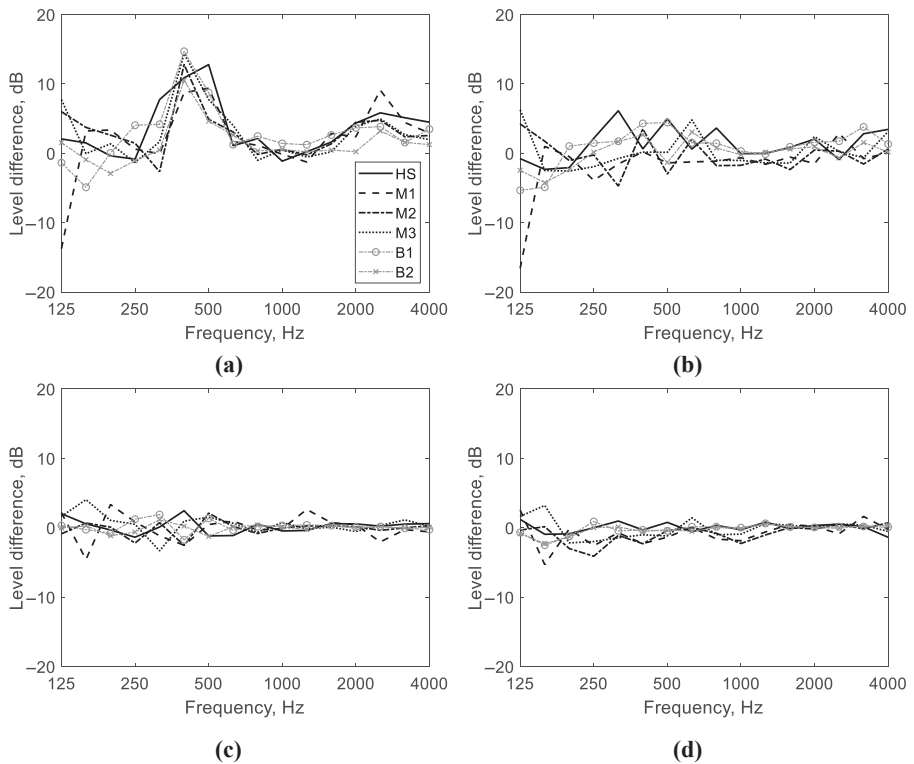


Figure 12.
Sound pressure level with the train body relative to the result without, for different train profiles – including ground effect

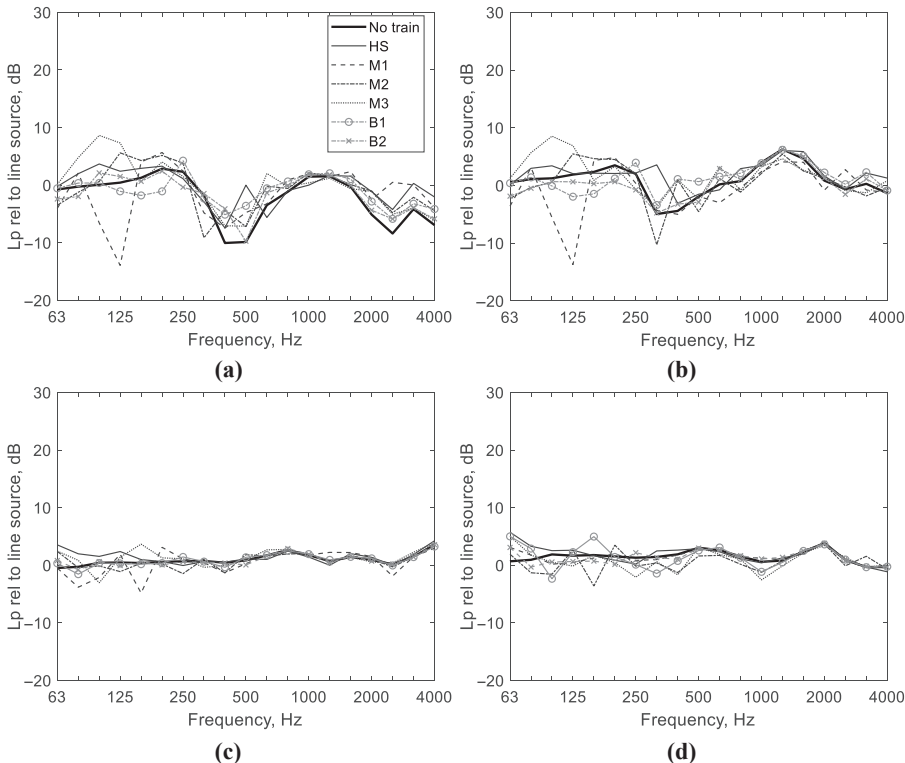
Note(s): (a) Rail vibrating vertically, 1.2 m receiver height; (b) rail vibrating vertically, 3.5 m receiver height; (c) rail vibrating laterally, 1.2 m receiver height; (d) rail vibrating laterally, 3.5 m receiver height
Source(s): Authors' own work

present, Figure 4, had a strong dip in the sound pressure, due to the predominantly vertical directivity, seen in Figure 9 (b); the presence of the train body then modifies this. For the receiver at 3.5 m height, Figure 12 (b), the level difference is mostly between -2 and $+3$ dB. For the radiation from the lateral vibration of the rail, the level differences are all close to 0 dB.

5. Assessment of line source estimates

Simple line source formulae, Equations (2) and (3), were introduced in Section 2.2. These give estimates of the relation between sound pressure level and sound power level for the rail. Here, the results obtained from the BE models including the train are compared with these line source formulae. To apply these formulae, the sound power level for the case *without* the train is used in Equations (2) and (3). Even though the train reduces the sound power from the rail (Figure 11), it does not significantly reduce the sound pressure component radiated towards the trackside (Figure 12).

Figure 13 shows the BE prediction of the sound pressure from the rail, normalized by the corresponding result from Equations (2) and (3); these results are for the case with no ground



Note(s): (a) Rail vibrating vertically, 1.2 m receiver height, normalised by Equation (2); (b) rail vibrating vertically, 3.5 m receiver height, normalised by Equation (2); (c) rail vibrating laterally, 1.2 m receiver height, normalised by Equation (3); (d) rail vibrating laterally, 3.5 m receiver height, normalised by Equation (3)

Source(s): Authors' own work

Figure 13. Sound pressure level from the rail, at 7.5 m distance, shown relative to the results for a line source – with no ground

reflection. The equivalent results with no train present are included for comparison. In the presence of the train, the results for vertical rail vibration are closer to 0 dB at mid and high frequencies. This suggests that the line source estimates can still be used in the presence of the train. Although the level at the dip at 300–500 Hz is increased, it is still around -5 dB; in addition, the peak at 1250 Hz in Figure 13 (b) is unaffected. The inclusion of the train has very little effect on the results for the lateral rail vibration, as seen earlier, and the level difference remains close to 0 dB.

Figure 14 shows the equivalent results obtained including the presence of the ground, based on using a flow resistivity of $3 \times 10^5 \text{ Pa.s/m}^2$. For the vertical rail vibration, the effect of including the train body is again to bring the estimates closer to 0 dB, that is, closer to the line source estimate. For the lateral rail vibration, peaks and dips appear due to the ground reflection, but the presence of the train does not affect them. In summary, these results demonstrate that the line source estimate with simple directivity can be used to approximate well the sound pressure from the rail in the presence of a train. This is valid for a wide range of train geometries tested.

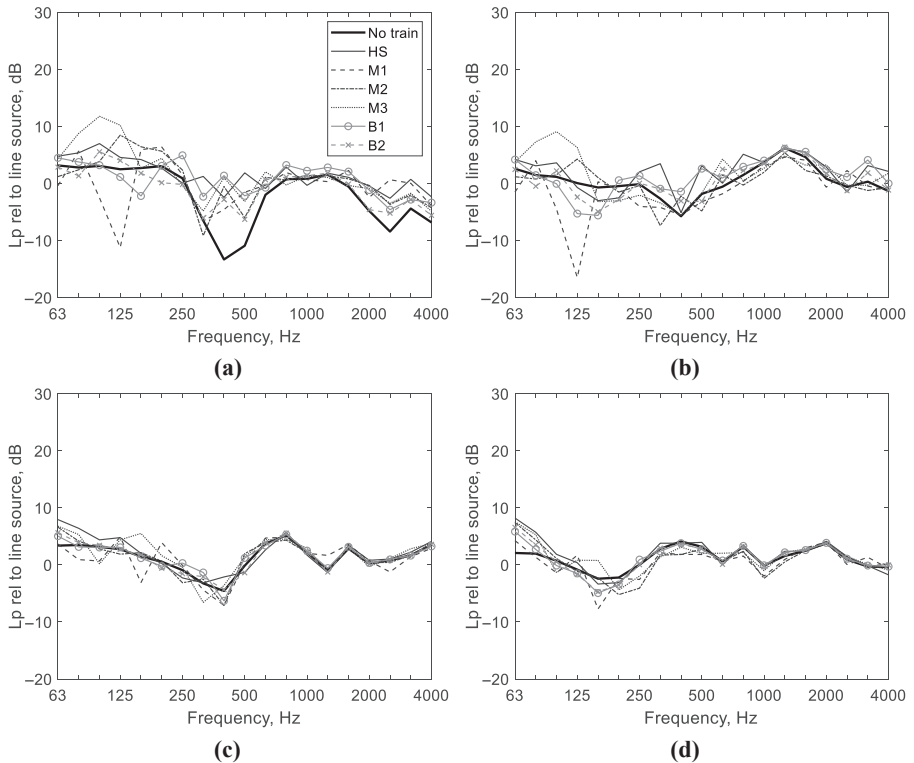


Figure 14. Sound pressure level from the rail, at 7.5 m distance, shown relative to the results for a line source – with ground effect

Note(s): (a) Rail vibrating vertically, 1.2 m receiver height, normalised by Equation (2); (b) rail vibrating vertically, 3.5 m receiver height, normalised by Equation (2); (c) rail vibrating laterally, 1.2 m receiver height, normalised by Equation (3); (d) rail vibrating laterally, 3.5 m receiver height, normalised by Equation (3)

Source(s): Authors' own work

6. Conclusions

The sound radiated by the rail vibration has been investigated using two-dimensional boundary element models, in order to study the influence of reflections from the ground and from the underside of the train. Comparisons with measurements on a metro train have also been presented. The main conclusions are:

- (1) Without the train present, the sound radiation from the rail occurs predominantly in the upper hemi-cylinder. The sound radiated toward the ground is shielded by the ballast shoulder, which has the effect of significantly reducing the ground reflection in the far field, especially for radiation from the vertical rail vibration.
- (2) The main consequence of introducing the train body is that sound is reflected back toward the track, especially for the vertical rail vibration. For ballasted tracks, as considered here, this sound is then partly absorbed by the ballast, reducing the sound power due to vertical vibration of the rail.
- (3) The presence of the train body causes an increase in the sound pressure at the trackside. The sound reflected from the bottom of the vehicle can also strengthen the ground reflection. The presence of the train body has negligible effect on the sound pressure level due to the lateral vibration of the rail.
- (4) The results from simple line source formulae agree well with the BE results for the radiation from the vertical vibration of the rail when the train body and the ground reflections are included. For the lateral rail vibration, the line dipole model agrees well with the BE results without the ground reflection, but the ground dip is still apparent in the results including the ground.

The main practical application of this work is that it allows the influence of the car body to be included in a simple but reliable way in predictions of rolling noise. It is also of importance in relation to experimental methods intended to separate wheel and rail contributions to rolling noise (Thompson *et al.*, 2018). The results presented here can be applied as corrections to allow the necessary vibro-acoustic transfer functions of the track to be measured without the train being present.

References

- Bender, E. K., & Remington, P. J. (1974). The influence of rails on train noise. *Journal of Sound and Vibration*, 37(3), 321–334. doi: [10.1016/s0022-460x\(74\)80248-8](https://doi.org/10.1016/s0022-460x(74)80248-8).
- Delany, M. E., & Bazley, E. N. (1970). Acoustical properties of fibrous absorbent materials. *Applied Acoustics*, 3(2), 105–116. doi: [10.1016/0003-682x\(70\)90031-9](https://doi.org/10.1016/0003-682x(70)90031-9).
- Dittrich, M., Letourneaux, F., & Jones, C. (2019). Source terms for railway noise prediction models – a new measurement standard. In *13th International Workshop on Railway Noise*, Ghent, Belgium, September 2019.
- Dragna, D., Blanc-Benon, P., & Poisson, F. (2014). Impulse propagation over a complex site: A comparison of experimental results and numerical predictions. *The Journal of the Acoustical Society of America*, 135(3), 1096–1105. doi: [10.1121/1.4864286](https://doi.org/10.1121/1.4864286).
- Fahy, F. (1995). The vibro-acoustic reciprocity principle and applications to noise control. *Acustica*, 81, 544–558.
- Han, J., He, Y., Wang, J., & Xiao, X. (2021). Simulation and experimental study on vibration and acoustic characteristics of a continuous supported embedded track. *Applied Acoustics*, 180, 108103. doi: [10.1016/j.apacoust.2021.108103](https://doi.org/10.1016/j.apacoust.2021.108103).
- Li, H., Thompson, D. J., Squicciarini, G., Liu, X., Rissmann, M., Denia, F., & Navarro, J. G. (2021). Investigation of acoustic transmission beneath a railway vehicle by using statistical energy

- analysis and an equivalent source model. *Mechanical Systems and Signal Processing*, 150, 107296. doi: [10.1016/j.ymssp.2020.107296](https://doi.org/10.1016/j.ymssp.2020.107296).
- Magrans, F. X. (1981). Method of measuring transmission paths. *Journal of Sound and Vibration*, 74(3), 321–330. doi: [10.1016/0022-460x\(81\)90302-3](https://doi.org/10.1016/0022-460x(81)90302-3).
- Nilsson, C.-M., & Jones, C. J. C. (2007). *Theory manual for WANDS 2.1, ISVR technical memorandum 975*. Southampton: University of Southampton.
- Nilsson, C.-M., Jones, C. J. C., Thompson, D. J., & Ryue, J. (2009). A waveguide finite element and boundary element approach to calculating the sound radiated by railway and tram rails. *Journal of Sound and Vibration*, 321(3-5), 813–836. doi: [10.1016/j.jsv.2008.10.027](https://doi.org/10.1016/j.jsv.2008.10.027).
- Petit, M.-F., Heckl, M., Bergemann, J., & Baae, J. (1992). Calculation of the radiation efficiency of railway rails using multipole synthesis. In *Proceedings DAGA 1992* (pp. 997–1000).
- Remington, P. J. (1976a). Wheel/rail noise-part I: Characterization of the wheel/rail dynamic system. *Journal of Sound and Vibration*, 46(3), 359–380. doi: [10.1016/0022-460x\(76\)90861-0](https://doi.org/10.1016/0022-460x(76)90861-0).
- Remington, P. J. (1976b). Wheel/rail noise-part IV: Rolling noise. *Journal of Sound and Vibration*, 46(3), 419–436. doi: [10.1016/0022-460x\(76\)90864-6](https://doi.org/10.1016/0022-460x(76)90864-6).
- Remington, P. J. (1987). Wheel/rail rolling noise I: Theoretical analysis. *The Journal of the Acoustical Society of America*, 81(6), 1805–1823. doi: [10.1121/1.394746](https://doi.org/10.1121/1.394746).
- Ryue, J., Jang, S., & Thompson, D. J. (2018). A wavenumber domain numerical analysis of rail noise including the surface impedance of the ground. *Journal of Sound and Vibration*, 432, 173–191. doi: [10.1016/j.jsv.2018.06.032](https://doi.org/10.1016/j.jsv.2018.06.032).
- Theysen, J. S. (2022). *Simulating rolling noise on ballasted and slab tracks: Vibration, radiation and pass-by signals*. PhD thesis. Gothenburg, Sweden: Chalmers University of Technology.
- Thompson, D. J. (1988). Predictions of acoustic radiation from vibrating wheels and rails. *Journal of Sound and Vibration*, 120(2), 275–280. doi: [10.1016/0022-460x\(88\)90435-x](https://doi.org/10.1016/0022-460x(88)90435-x).
- Thompson, D. J. (2009). *Railway noise and vibration mechanisms, modelling and means of control*. Oxford: Elsevier.
- Thompson, D. J., Hemsforth, B., & Vincent, N. (1996a). Experimental validation of the TWINS prediction program for rolling noise, Part 1: Description of the model and method. *Journal of Sound and Vibration*, 193(1), 123–135. doi: [10.1006/jsvi.1996.0252](https://doi.org/10.1006/jsvi.1996.0252).
- Thompson, D. J., Fodiman, P., & Mahé, H. (1996b). Experimental validation of the TWINS prediction program for rolling noise, part 2: Results. *Journal of Sound and Vibration*, 193(1), 137–147. doi: [10.1006/jsvi.1996.0253](https://doi.org/10.1006/jsvi.1996.0253).
- Thompson, D. J., Jones, C. J. C., & Turner, N. (2003). Investigation into the validity of two-dimensional models for sound radiation from waves in rails. *The Journal of Acoustical Society of America*, 113(4, Pt 1), 1965–1974. doi: [10.1121/1.1555612](https://doi.org/10.1121/1.1555612).
- Thompson, D. J., Squicciarini, G., Zhang, J., Arteaga, I. L., Zea, E., Dittrich, M., . . . Wändell, J. (2018). Assessment of measurement-based methods for separating wheel and track contributions to railway rolling noise. *Applied Acoustics*, 140, 48–62. doi: [10.1016/j.apacoust.2018.05.012](https://doi.org/10.1016/j.apacoust.2018.05.012).
- Thompson, D. J., Dittrich, M. G., Jansen, H. W., Zhao, D., & Cierco, E. (2022). Track and vehicle separation and transposition techniques including theoretical description and proposal for full scale validation test campaign. Shift2Rail/H2020 project TRANSIT, grant agreement no. 881771, Deliverable D3.2.
- Van Lier, S. (2000). The vibro-acoustic modelling of slab track with embedded rails. *Journal of Sound and Vibration*, 231(3), 805–817. doi: [10.1006/jsvi.1999.2564](https://doi.org/10.1006/jsvi.1999.2564).
- Wu, T. W. (2000). *Boundary element acoustics: Fundamentals and computer codes*. Southampton: WIT Press.
- Zhang, X. (2010). The directivity of railway noise at different speeds. *Journal of Sound and Vibration*, 329(25), 5273–5288. doi: [10.1016/j.jsv.2010.07.003](https://doi.org/10.1016/j.jsv.2010.07.003).

- Zhang, X., & Jonasson, H. G. (2006). Directivity of railway noise sources. *Journal of Sound and Vibration*, 293(3-5), 995–1006. doi: [10.1016/j.jsv.2005.08.057](https://doi.org/10.1016/j.jsv.2005.08.057).
- Zhang, X., Squicciarini, G., & Thompson, D. J. (2016). Sound radiation of a railway rail in close proximity to the ground. *Journal of Sound and Vibration*, 326, 111–124. doi: [10.1016/j.jsv.2015.10.006](https://doi.org/10.1016/j.jsv.2015.10.006).
- Zhang, X., Thompson, D. J., Quaranta, E., & Squicciarini, G. (2019). An engineering model for the prediction of the sound radiation from a railway track. *Journal of Sound and Vibration*, 461, 114921. doi: [10.1016/j.jsv.2019.114921](https://doi.org/10.1016/j.jsv.2019.114921).

Corresponding author

David J. Thompson can be contacted at: djt@isvr.soton.ac.uk

For instructions on how to order reprints of this article, please visit our website:

www.emeraldgrouppublishing.com/licensing/reprints.htm

Or contact us for further details: permissions@emeraldinsight.com